Chemical Science

ROYAL SOCIETY OF CHEMISTRY

EDGE ARTICLE

View Article Online
View Journal | View Issue

Cite this: *Chem. Sci.*, 2025, **16**, 6014

All publication charges for this article have been paid for by the Royal Society of Chemistry

Received 25th September 2024
Accepted 27th February 2025

DOI: 10.1039/d4sc06481j

rsc.li/chemical-science

A bacteria-based bioorthogonal platform disrupts the flexible lipid homeostasis for potent metabolic therapy†

Jiadai Yi,[ab] Huan Wang,[*a] Qingqing Deng,[ab] Congcong Huang,[ab] Lu Zhang,[a] Mengyu Sun,[ab] Jinsong Ren[*ab] and Xiaogang Qu[*ab]

Cancer cells exhibit altered metabolism and energetics, prominently reprogramming lipid metabolism to support tumor growth and progression, making it a promising target for cancer therapy. However, traditional genetic and pharmaceutical approaches for disrupting lipid metabolism face challenges due to the adaptability of tumor metabolism and potential side effects on normal tissues. Here, we present a bacteria-based bioorthogonal platform combining transition metal catalysts and *Lactobacillus* to disrupt the flexible lipid homeostasis in tumors. This platform activates glutamine transporter inhibitors *in situ*, targeting lipid synthesis in hypoxic tumor environments, while *Lactobacillus* inhibits lipid accumulation. By disrupting lipid metabolism and glutamine utilization, the present study proposes a safe and potent strategy for cancer therapy, with potential applications for other metabolic diseases.

Introduction

Altered cellular metabolism and energetics are central features of cancer cells.[1,2] Multiple pathways and mechanisms are involved in altering the cellular utilization of various metabolites and molecules, thereby supporting aberrant cellular replication, dissemination from the primary tumor, establishment of secondary tumors, and immune evasion.[3] Within these adaptations, reprogramming of lipid metabolism plays a driving role in promoting tumorigenesis and cancer progression.[4] A majority of tumor cells exhibit significant alterations in their lipid signatures.[4] Tumor cells can enhance *de novo* lipogenesis, increase fatty acid uptake, and promote fatty oxidation to produce energy and accumulate lipids. The elevated lipid metabolism in cancer cells is primarily driven by the increased demand for lipids to synthesize plasma membranes and generate energy.[3] Besides, the elevated lipid metabolism defines tumor progression and resistance to different therapies by stimulating tumor-promoting inflammation, enhancing angiogenesis, influencing stromal cells, and even enabling immune evasion by drastically affecting the immune cell compartment.[5–8] Therefore, targeting lipid metabolism offers new therapeutic opportunities and has attracted much attention in developing various inhibitors for cancer therapy.

To date, genetic manipulations and pharmaceutical interventions have been used to disturb lipid metabolism for cancer therapy.[9–12] However, emerging evidence has revealed that lipid metabolism is highly flexible in the tumor microenvironment. Cancer cells in hypoxia regions are compensate by converting alternative carbon sources for fatty acid biosynthesis, wherein glutamine serves as one of the main sources for fatty acid synthesis.[13,14] As a result, several inhibitors have been developed to suppress the uptake or synthesis of glutamine for cancer therapy.[15–18] Yet, the risk of side effects of drugs on normal cell populations and specific organs limits the applicable dosages. For example, glutamate transporter dysfunction is associated with neurodegenerative diseases (*e.g.* amyotrophic lateral sclerosis, Alzheimer's disease) and ischemic damage (*e.g.* after a stroke).[19] Besides, most of these strategies remain limited by either insufficient accumulation in targeting tumor sites or complex synthesis procedures and are thus still in the preclinical "tool compound" stage.

Recently, the advancement of bioorthogonal chemistry has driven innovations in toolkits for the *in situ* generation of imaging and therapeutic agents in complex biological systems.[20–27] Among them, the utilization of transition metal catalysts (TMCs) for specific drug activation within living systems is considered a promising strategy, offering the potential to avoid non-targeted toxicity and mitigate adverse reactions in disease treatment.[28–31] Recently, utilizing transition metals-loaded nanoparticles in bioorthogonal prodrug activation has effectively mitigated the systemic toxicity associated with metal complexes, primarily due to their instability and

[a]*Laboratory of Chemical Biology and State Key Laboratory of Rare Earth Resource Utilization, Changchun Institute of Applied Chemistry, Chinese Academy of Sciences, Changchun, Jilin 130022, P. R. China. E-mail: huanwang@ciac.ac.cn; jren@ciac.ac.cn; xqu@ciac.ac.cn*

[b]*School of Applied Chemistry and Engineering, University of Science and Technology of China, Hefei, Anhui 230026, P. R. China*

† Electronic supplementary information (ESI) available. See DOI: https://doi.org/10.1039/d4sc06481j

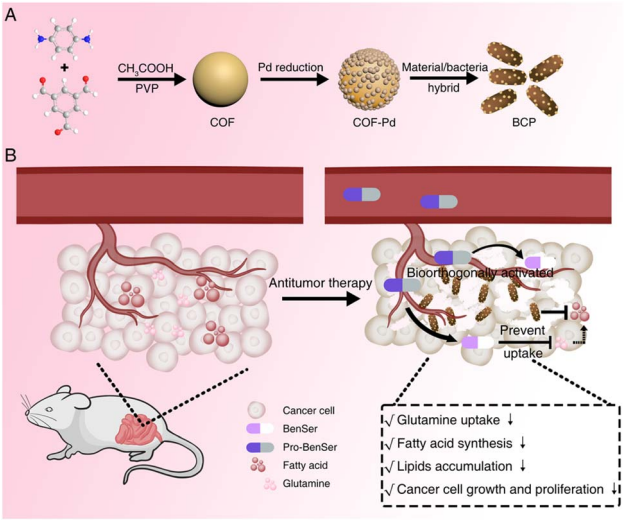

Fig. 1 (A) and (B) Schematic illustration of the design of the bioorthogonal catalytic platform based on bacteria and its mode of action.

unpredictable side effects.[32] On the other hand, the virtue of specific bacteria has led to numerous unanticipated accomplishments in various fields, including chemicals production,[33,34] microbial fuel cells (MFCs),[35–37] biosensing, and disease treatment,[38–42] garnering considerable interest. Advancements in nanotechnology and surface modification techniques have enhanced the functional diversity of bacterial therapies, thereby improving their therapeutic efficacy and clinical translation potential.[43–45] As dominant representatives of probiotics, *Lactobacillus* has been proven to stimulate lipolysis and inhibit lipogenesis to ameliorate high-fat diet-induced hyperlipidemia and diabetes.[46–49] Capitalizing on these advantages of transition metal catalysts and *Lactobacillus*, herein, a bacteria-based bioorthogonal platform was constructed to disrupt the flexible lipid homeostasis for potent metabolic therapy for the first time (Fig. 1). Specifically, the bioorthogonal catalyst (Pd^0) with excellent catalytic activity can activate the glutamine transporter inhibitors *in situ*, which intercept the source of lipid synthesis of tumor cells under hypoxia conditions. Meanwhile, the anaerobic *Lactobacillus* can selectively colonize into the hypoxia tumor site and inhibit lipids accumulation. The hybrid platform disrupts lipid homeostasis by intercepting lipid synthesis and accumulation through multifaceted approaches. Moreover, as the dominant energy source, the glutamine metabolism of cancer cells was also intercepted for synergistic tumor therapy. Taken together, we believe that this bacteria-based bioorthogonal platform could be an outstanding non-toxic candidate for cancer therapy and provide a new strategy for the treatment of other metabolic diseases in the future.

Results and discussion

As depicted in Fig. 1A, the bacteria-based bioorthogonal platform underwent a three-step preparation process. In the first step, the relatively uniform-sized spherical covalent-organic frameworks (COF) with a diameter of approximately 150 nm were successfully prepared, as indicated by scanning electron microscopy (SEM) images (Fig. 2A).[50] During the second step, the COF was used as a scaffold to stabilize ultrafine (~3 nm) palladium (Pd) nanoparticles (Pd^0) synthesized *via in situ* reduction, forming COF–Pd composites (denoted as CP) nanoparticles (Fig. 2B–D and S1†).[51] Through cell-compatible amidation reactions, functional components can be conjugated to the bacterial surface for loading and functionalization.[43] At the final stage, the bacteria–COF–Pd composites (denoted as BCP) were synthesized by incubating CP with bacteria at room temperature according to previously reported approaches with modifications (Fig. 2E).[52] As illustrated in Fig. S2,† the combination of CP with bacteria has almost no toxic effect on bacterial growth. The mapping images and energy-dispersive spectrum (EDS) demonstrated the uniform distributions of C, N, O, and Pd elements throughout the entire architecture of BCP (Fig. 2F and S3†). The results of dynamic light scattering (DLS) revealed that both COF and CP exhibit similar average hydrodynamic diameters. In contrast, the average hydrodynamic size of BCP with bacteria binding is much larger (>1000 nm) as shown in Fig. 2G. The Pd content in BCP was further determined to be 0.5 wt% by inductively coupled plasma mass spectrometry (ICP-MS). Furthermore, additional characterizations were conducted including Fourier transform infrared spectroscopy (FTIR), ζ potential measurement, transmission electron microscopy (TEM), X-ray diffraction (XRD), and X-ray photoelectron spectroscopy (XPS). Upon binding with bacteria, there was a notable decrease in the ζ potential of the CP (Fig. 2H). Compared to CP, BCP exhibits an additional peak at 1050 cm^{-1}, which is attributed to the bending vibrations of the C–O bonds in the carboxyl groups on the bacterial surface (Fig. S4†).[53] In the HR-TEM images, the lattice spacing of the (111) facet of Pd (JCPDS card no. 46-1043) is consistent with the corresponding XRD patterns (Fig. S5 and S6†). XPS analysis indicated that palladium was primarily in the form of Pd^0, with a small amount of Pd^{II} species (Fig. 2I and J).[54]

To investigate the catalytic activity of BCP, the cleavage of the allylcarbamate group in the fluorescent precursor *N*-allyloxycarbonyl coumarin (*N*-alloc-coumarin) was employed as a representative reaction (Fig. 3A). As depicted in Fig. 3B and S7,† in comparison to the control group, the increase in fluorescence intensity at 450 nm of *N*-alloc-coumarin after incubating with CP and BCP indicated that both CP and BCP had admirable catalytic capacity. Particularly, in the presence of the same content of Pd, the catalytic efficiency of BCP is slightly higher than that of CP. The difference in catalytic efficiency between CP and BCP might be attributed to the variations in their dispersibility (Fig. S8 and S9†) as shown in Fig. 3C and D, under the same concentration condition of Pd, the fluorescence intensity increased with the extension of the incubation time of fluorescent precursors and BCP. Subsequently, the products in the supernatant of the reaction systems were analyzed by high-performance liquid chromatography (HPLC). As shown in Fig. S10,† BCP could catalyze the cleavage of *N*-alloc coumarin in a time-dependent manner As shown in Fig. 3E, F, and S11,† the yield of the catalytic reaction increases with incubation

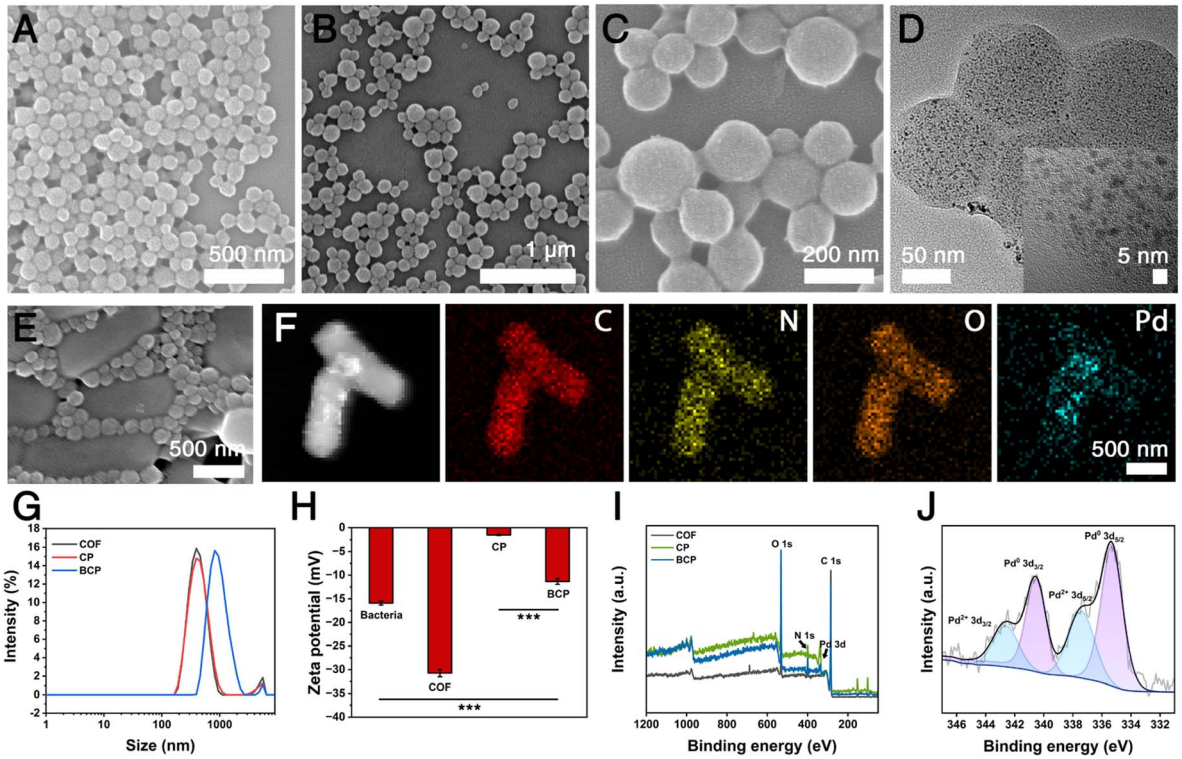

Fig. 2 (A) SEM image of COF. (B and C) SEM image of CP. (D) TEM image of CP. (E) SEM image of BCP. (F) STEM-HAADF images and corresponding elemental mapping images of BCP. (G) Dynamic light scattering results of COF, CP, and BCP. (H) ζ potentials of bacteria, COF, CP, and BCP. (I) XPS survey spectra of COF, CP, and BCP. (J) High-resolution Pd 3d XPS spectra of the BCP.

time, exceeding 80% after 24 hours. With the same incubation time, BCP could catalyze the cleavage of *N*-alloc coumarin in a concentration-dependent manner as shown in Fig. 3G. Furthermore, we performed a time-dependent analysis of the BenSer release in the buffer system using HPLC technology, as shown in Fig. S12.† The observed conversion efficiency of Pro-BenSer was generally consistent with that of pro-coumarin. Additionally, the SEM images of BCP post-reaction and after storage for a period of time are depicted in Fig. S13 and S14,† exhibit relatively intact morphology. Elemental analysis of the supernatant indicates that metal release is negligible across diverse systems, suggesting that the catalyst maintains a certain degree of stability (Fig. S15†). The successful cleavage reaction in the vial has laid the foundation for the subsequent biomedical application of BCP catalytic activation reaction.

Next, we investigated the catalytic performance of the platform *in vitro* on CT26 cells, a murine colon carcinoma cell line. Before evaluating the catalytic performance of BCP, a comprehensive assessment of its cytotoxicity was conducted by the methyl thiazolyl tetrazolium (MTT) method. In the range of 0 to 100 μg mL^{-1}, BCP showed negligible cytotoxicity towards normal cells 3T3 (embryonic fibroblast) (Fig. S16†), indicating that BCP exhibited high biocompatibility. Subsequently, cells were divided into four groups, and defined as the control (cells alone), cells treated with BCP alone, cells treated with the fluorescent precursor alone, and cells treated with both BCP and the fluorescent precursor. The changes in cellular fluorescence intensity were then assessed using confocal laser scanning microscopy (CLSM). After co-incubation for a certain period, we could observe that the CT26 cells in these groups subjected to different treatments did not show noticeable morphological changes. The groups that were treated with either the fluorescent precursor or the catalyst alone did not exhibit detectable fluorescence signals. In comparison to the other groups, the cells treated with both the fluorescent precursor and BCP showed bright blue fluorescence (Fig. 4A), indicating the deprotection of the caged fluorescent precursor catalyzed by the BCP. As anticipated, the flow cytometry analysis was further conducted to reverify the above results, and the analysis of the average fluorescence intensity showed an intracellular catalytic efficiency of approximately 70% (Fig. 4B and C). All these discoveries indicated that BCP could act as effective bioorthogonal catalysts *in vitro*.

Encouraged by the high catalytic activity of BCP *in vitro*, CT26 cells were thereafter selected as a model cell line to investigate the intracellular prodrug conversion capability of the BCP platform. Benzylserine (BenSer) has emerged as a potent inhibitor of cancer cell growth by modulating the expression and activity of key amino acid transporters, including ASCT2, disrupting intracellular amino acid homeostasis and triggering amino acid response pathways.[19,55] The inhibition of glutamine uptake by BenSer leads to decreased cell viability and impaired cell cycle progression. Nevertheless, the potential side effects on normal cell populations and specific organs restrict the dosages

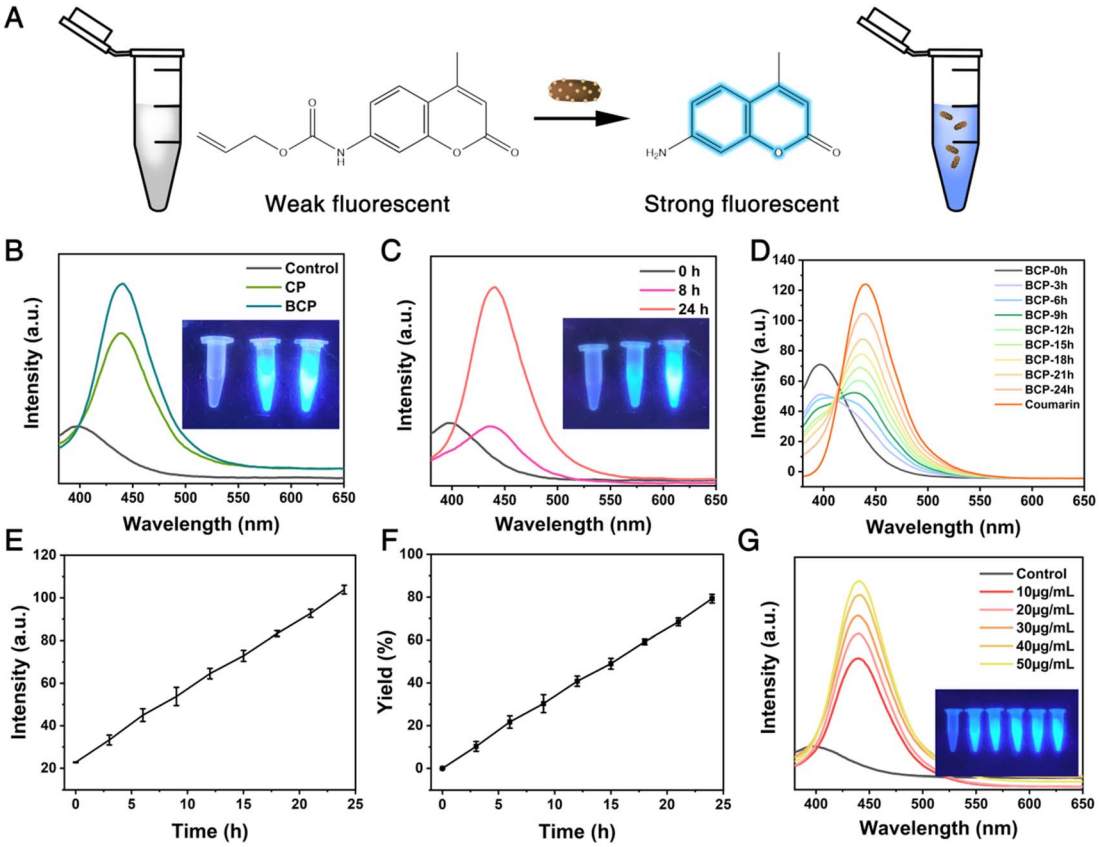

Fig. 3 (A) Schematic illustration of the allylcarbamate cleavage of *N*-alloc coumarin catalyzed by BCP NPs. (B) The fluorescence spectra of pro-coumarin cleavage reaction catalyzed by CP or BCP with the same Pd concentration. (C) The fluorescence changes and photograph (inset) of the pro-coumarin cleavage reaction catalyzed by BCP at the same concentration after 8 and 24 hours. (D) The fluorescence spectra of the cleavage of the pro-coumarin catalyzed by BCP (20 μg mL^{-1}) at the same concentration were monitored continuously over 24 hours. (E) Time-dependent changes in fluorescence intensity of the reaction of the fluorescent precursor catalyzed by BCP from 0 to 24 hours. Data are presented as mean ± SD ($n = 3$). (F) The reaction time-dependent-yield corresponds to Fig. 2E. (G) The fluorescence spectra of pro-coumarin cleavage reaction catalyzed by BCP NPs with different Pd concentrations.

at which these drugs can be applied. Structurally, the serine moiety in BenSer is crucial for its activity. Based on this, it was hypothesized that blocking the amine group might inhibit BenSer's activity by preventing its interaction with target receptors. To test this hypothesis, an allyloxycarbonyl group was introduced to cage the amine, resulting in the development of

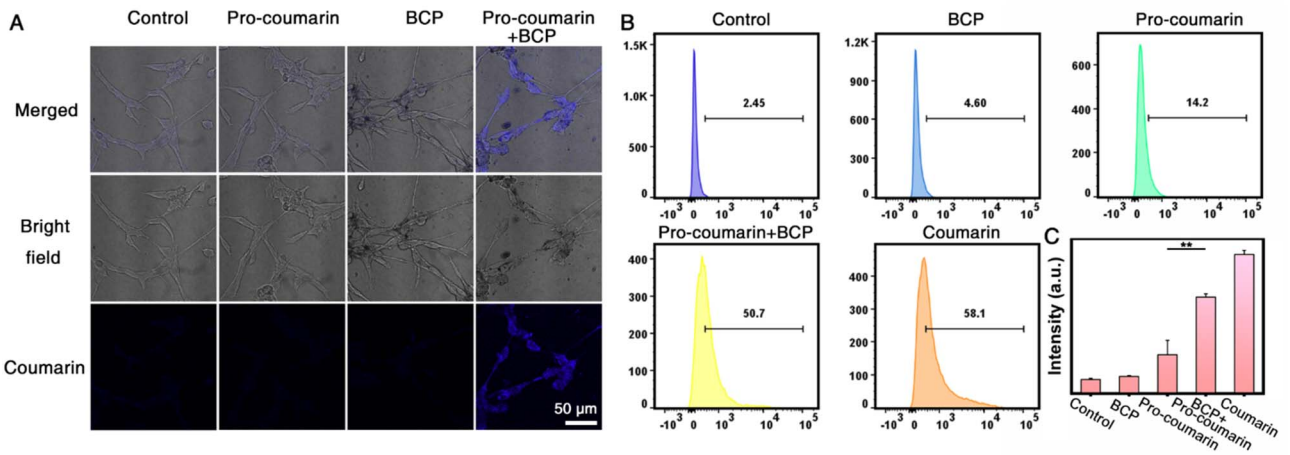

Fig. 4 BCP can act as effective biorthogonal catalysts *in vitro*. (A) The fluorescence images of CT26 cells after various treatments. (B) Quantitative analysis of fluorescence intensity in the fluorescence images in various experimental groups in the presence of the fluorescent precursor. (C) The flow cytometry analysis of fluorescence changes in various experimental groups for different treatment groups. Data are presented as mean ± SD ($n = 3$).

the palladium-labile prodrug, Pro-BenSer (PB). This prodrug aims to regulate BenSer's activity through controlled release, potentially enhancing its therapeutic efficacy in cancer treatment. The cytotoxicity of PB and BenSer was assessed using the MTT assay. As shown in Fig. 5A and S17,† the MTT results revealed a dose-dependent cytotoxicity of BenSer, while the PB showed high biocompatibility even at a concentration of 20 mM. Hypoxic cancer cells utilize alternative carbon sources for fatty acid biosynthesis, with glutamine being one of the primary sources for fatty acid synthesis.[13] Therefore, inhibiting glutamine uptake can further reduce the fatty acid content within the cells. Based on this, we measured the changes in intracellular glutamine levels following different treatments. The results showed that the PB + BCP treatment group exhibited the lowest intracellular glutamine levels among all groups (Fig. S18†). Moreover, the relative intracellular glutamine levels in the PB + BCP treatment group decreased over time (Fig. S19†). We then evaluated the intracellular free fatty acid (FFA) consumption capacity of PB + BCP *in vitro*. Compared with the control group, the FFA concentration in the PB + BCP treatment group showed a significant decrease. It could be observed that the group of BCP alone and the group of PB + CP also have a certain consumption of FFA (Fig. 5B). According to previous literature reports, one of the reasons for the reduction in FFA caused by BCP treatment may be due to the increased catabolism of fatty acids by lactic acid bacteria, which reduces their accumulation. At the same time, compared with the group of BCP alone or PB + CP, the PB + BCP group showed significantly higher cell-killing potential. Next, the live/dead staining of CT26 cells was analyzed by CLSM, as depicted in Fig. 5C. Cells co-incubated with the catalyst BCP and PB displayed a noticeable decrease in green fluorescence signal and a prominent increase in red fluorescence signal, indicating the significant cytotoxicity caused by PB + BCP. This is likely due to the combined action of our catalyst and the activated drug, leading to disruptions in lipid metabolism. Additionally, the PB + BCP treatment exhibited superior cytotoxicity compared to the PB + CP treatment. The above results indicated that PB was catalytically converted to BenSer by the catalyst, leading to obvious cytotoxicity. Next, we also investigated the cell cytotoxicity by using flow cytometry to assess the cellular apoptotic level, which further indicated the cytotoxicity of PB + BCP treatment (Fig. 5D). Based on the above results, it could be evident that the catalyst could be further employed for prodrug activation for tumor therapy *in vivo*.

Encouraged by the significant anti-proliferative efficacy observed *in vitro*, we proceeded to evaluate the antitumor efficiency of our designed bacteria-based bioorthogonal platform *in vivo* on CT26 tumor-bearing mice. The *in vivo* biosafety of both the catalyst BCP and prodrug PB was investigated in detail. Hemolysis analysis showed that the catalyst did not cause significant hemolysis, indicating good biocompatibility (Fig. S20†). The injection of BCP or PB also had no obvious influence on the bodyweight changes of the experimental mice (Fig. S21†). Blood biochemistry and hematological analysis, as well as hematoxylin and eosin (H&E) staining images of the

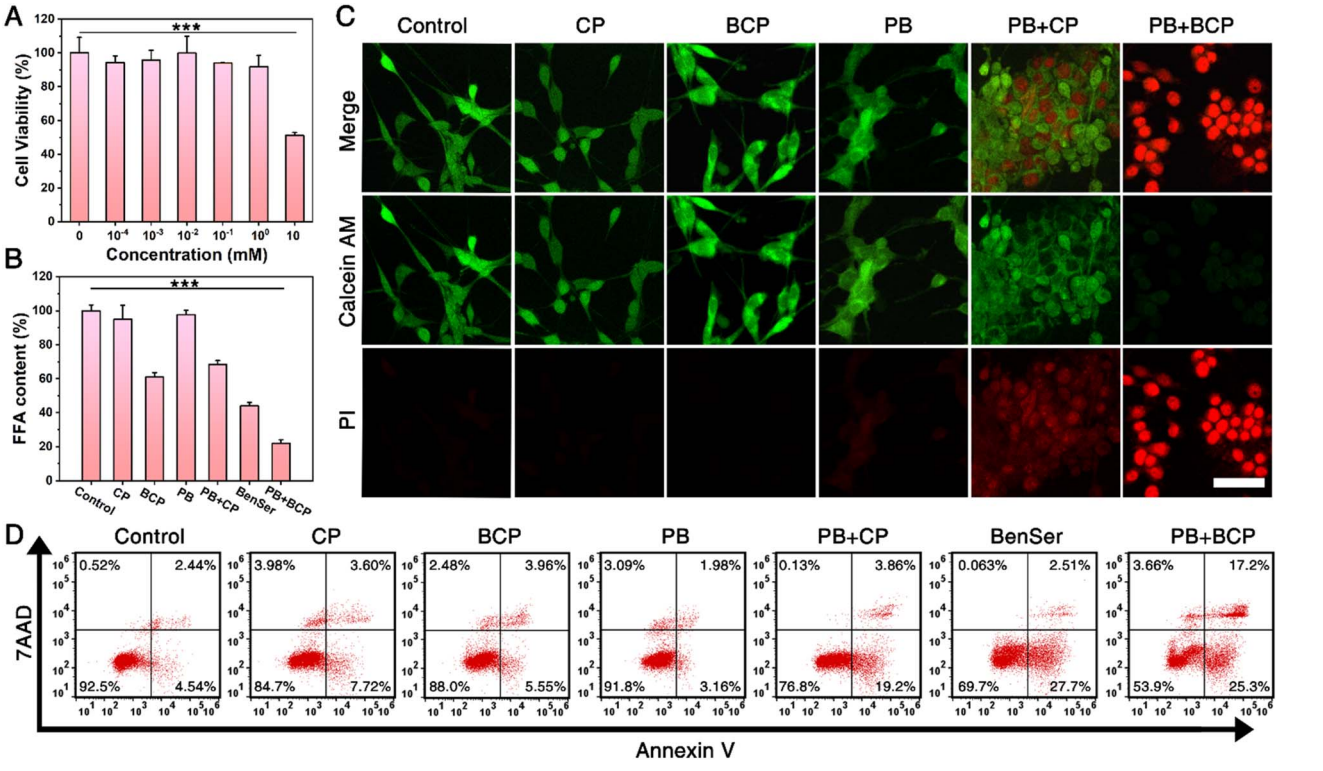

Fig. 5 (A) Cell viability of CT26 cells with different concentrations of BenSer. (B) FFA levels of CT26 cells after different treatments. Data were presented as mean ± SD ($n = 3$). (C) Live/dead staining images of CT26 cells after different treatments. The scale bar is 50 μm. (D) Flow cytometry analysis of the apoptotic proportion of CT26 cells *via* Annexin V-FITC/7-AAD.

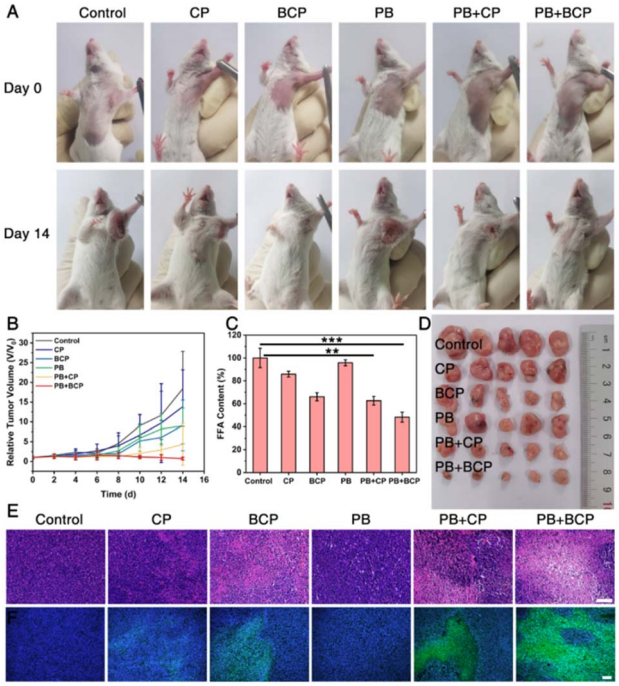

Fig. 6 *In vivo* antitumor efficacy. (A) Photographs of the CT26 tumor-bearing mice in different experimental groups on day 0 and day 14. (B) Changes in tumor volumes after various treatments ($n = 5$). (C) Tumor FFA content after various treatments on day 14 ($n = 4$). (D) Photographs of the dissected tumors after various treatments on day 14. (E) H&E-staining images of the tumors of mice in various experimental groups. Scale bars is 50 μm. (F) TUNEL-staining images of the tumors of mice in various experimental groups. Scale bar is 100 μm. Data are presented as mean ± SD ($n = 5$).

major organs (heart, liver, spleen, lung, and kidney) further confirm the satisfactory biocompatibility of PB or BCP (Fig. S22 and S23†). Subsequently, the therapeutic effect of the bacteria-based bioorthogonal platform was evaluated on CT26 tumor-bearing mice. The mice were divided into six groups: (1) control group; (2) CP; (3) BCP; (4) PB, (5) PB + CP, and (6) PB + BCP (Fig. 6A). Each treatment group was treated every other day (Fig. S24†). Negligible bodyweight changes could be observed in all groups during the experimental period (Fig. S25†). The relative tumor volume curves were recorded as shown in Fig. 6B. Both photographs and the calculated tumor volumes showed rapid tumor growth in the control, prodrug, and CP groups, indicating minimal antitumor effects of PB or CP alone. In contrast, the BCP, PB + CP, and PB + BCP groups exhibited significant tumor growth inhibition, with the PB + BCP combination showing the most pronounced effect (Fig. 6B and D).

We hypothesize that the better antitumor efficacy of the BCP bioorthogonal platform combined with prodrug activation was due to the simultaneous disruption of lipid homeostasis at the tumor site by drugs and bacteria. Therefore, we evaluated the level of FFA in tumor tissues. As depicted in Fig. 6C, the group treated with the PB + BCP combination exhibited a significant decrease in FFA level in the tumor tissue. These findings further support the antitumor mechanism of our bacteria-based bioorthogonal platform. On the one hand, bacteria proliferate at the tumor site, consuming the nutrients and modulating the lipid metabolism levels; on the other hand, the de-protected prodrug inhibits glutamine uptake, further suppressing lipid synthesis. In addition, to assess the pathological damage of the tumor and the level of apoptosis, H&E staining and terminal deoxynucleotide transferase dUTP notch labeling (TUNEL) staining were performed. As shown in Fig. 6E, the BCP group and PB + CP group were moderately damaged, while the tumor cells in the PB + BCP group were severely damaged, further verifying the BCP-mediated synergistic effect. In addition, histological analysis of major organs after treatment in the catalyst and prodrug group indicated no detectable damage or side effects of the bacteria-based bioorthogonal platform (Fig. S26†), demonstrating the high biocompatibility of the bio-intercepter. Overall, the above experimental results demonstrated that this bacteria-based bioorthogonal platform had satisfactory antitumor efficacy.

Conclusions

In summary, a bacteria-based bioorthogonal platform (BCP) has been developed and successfully applied in cancer therapy. In this design, BCP not only generates the glutamine transporter inhibitor (BenSer) by bioorthogonal catalytic decaging but also inhibits lipid accumulation at the tumor site through its metabolism. Such dual action disrupts lipid homeostasis in multiple ways, realizing effective metabolic therapy. The *in situ* activation of BenSer in tumors enhances its bioavailability and minimizes toxicity to normal tissues. As an example of a bacteria-based bioorthogonal platform, this study leverages bacterial and bioorthogonal chemistry to tackle the challenge of flexible lipid metabolism in tumor therapy, offering a promising approach for the treatment of other metabolic diseases in the future.

Ethical statement

All animal procedures were performed in accordance with the Guidelines for Care and Use of Laboratory Animals of Changchun Institute of Applied Chemistry Chinese Academy of Sciences and approved by Institutional Animal Care and Use Committee of Changchun Institute of Applied Chemistry Chinese Academy of Sciences (Permit Number: 20210016).

Data availability

The data supporting this article have been included as part of the ESI.†

Author contributions

J. Y., H. W., J. R., and X. Q. conceived and designed the study. J. Y. performed the synthesis of the bioorthogonal platform. J. Y., C. H., and L. Z. performed the synthesis of the prodrug. J. Y. and Q. D. performed the characterization of the bioorthogonal platform. J. Y., Q. D., and M. S. performed the cell culture

studies. J. Y. and C. H. assisted with the animal studies. All the authors analyzed the experimental data and wrote the paper. H. W., J. R., and X. Q. supervised the whole project.

Conflicts of interest

There are no conflicts to declare.

Acknowledgements

This work was supported by the Science and Technology Development Project of Jilin Province (20230101040JC), the National Key R&D Program of China (2021YFF1200700 and 2022YFA1205804), the National Natural Science Foundation of China (22437006, T2495262, 22475210, 22237006), and the Jilin Province Youth Scientific and Technological Talent Support Project (QT202403).

Notes and references

1 D. Hanahan and R. A. Weinberg, Hallmarks of Cancer: The Next Generation, *Cell*, 2011, **144**, 646–674.
2 L. Y. Bai, F. Q. Bu, X. J. Li, S. T. Zhang and L. Min, Mass spectrometry-based extracellular vesicle micromolecule detection in cancer biomarker discovery: An overview of metabolomics and lipidomics, *View*, 2023, **4**, 20220086.
3 L. A. Broadfield, A. A. Pane, A. Talebi, J. V. Swinnen and S. M. Fendt, Lipid metabolism in cancer: New perspectives and emerging mechanisms, *Dev. Cell*, 2021, **56**, 1363–1393.
4 S. Beloribi-Djefaflia, S. Vasseur and F. Guillaumond, Lipid metabolic reprogramming in cancer cells, *Oncogenesis*, 2016, **5**, e189.
5 Y. Hisano and T. Hla, Bioactive lysolipids in cancer and angiogenesis, *Pharmacol. Ther.*, 2019, **193**, 91–98.
6 V. Chiurchiù, A. Leuti and M. Maccarrone, Bioactive Lipids and Chronic Inflammation: Managing the Fire Within, *Front. Immunol.*, 2018, **9**, 38.
7 S. Zelenay, A. G. van der Veen, J. P. Böttcher, K. J. Snelgrove, N. Rogers, S. E. Acton, P. Chakravarty, M. R. Girotti, R. Marais, S. A. Quezada, E. Sahai and C. R. E. Sousa, Cyclooxygenase-Dependent Tumor Growth through Evasion of Immunity, *Cell*, 2015, **162**, 1257–1270.
8 A. E. Baek, Y. R. A. Yu, S. S. He, S. E. Wardell, C. Y. Chang, S. Kwon, R. V. Pillai, H. B. McDowell, J. W. Thompson, L. G. Dubois, P. M. Sullivan, J. K. Kemper, M. D. Gunn, D. P. McDonnell and E. R. Nelson, The cholesterol metabolite 27 hydroxycholesterol facilitates breast cancer metastasis through its actions on immune cells, *Nat. Commun.*, 2017, **8**, 864.
9 Y. J. Zhao, X. Liu, F. S. Si, L. Huang, A. Q. Gao, W. L. Lin, D. F. Hoft, Q. X. Shao and G. Y. Peng, Citrate Promotes Excessive Lipid Biosynthesis and Senescence in Tumor Cells for Tumor Therapy, *Adv. Sci.*, 2022, **9**, e2101553.
10 S. S. Wu, J. J. Wang, Z. Fu, G. Familiari, M. Relucenti, M. Aschner, X. B. Li, R. Chen and H. Q. Chen, Matairesinol Nanoparticles Restore Chemosensitivity and Suppress Colorectal Cancer Progression in Preclinical Models: Role of Lipid Metabolism Reprogramming, *Nano Lett.*, 2023, **23**, 1970–1980.
11 J. Zhou, J. C. Ji, X. Li, Y. X. Zhang, L. Gu, X. L. Zheng, Y. K. Li, J. H. He, C. Yang, K. Xiao, Q. Y. Gong, Z. W. Gu and K. Luo, Homomultivalent Polymeric Nanotraps Disturb Lipid Metabolism Homeostasis and Tune Pyroptosis in Cancer, *Adv. Mater.*, 2024, **36**, 2312528.
12 M. Oh, S. Y. Jang, J. Y. Lee, J. W. Kim, Y. Jung, J. Kim, J. Seo, T. S. Han, E. Jang, H. Y. Son, D. Kim, M. W. Kim, J. S. Park, K. H. Song, K. J. Oh, W. K. Kim, K. H. Bae, Y. M. Huh, S. H. Kim, D. Kim, B. S. Han, S. C. Lee, G. S. Hwang and E. W. Lee, The lipoprotein-associated phospholipase A2 inhibitor Darapladib sensitises cancer cells to ferroptosis by remodelling lipid metabolism, *Nat. Commun.*, 2023, **14**, 5728.
13 F. Röhrig and A. Schulze, The multifaceted roles of fatty acid synthesis in cancer, *Nat. Rev. Cancer*, 2016, **16**, 732–749.
14 B. J. Altman, Z. E. Stine and C. V. Dang, From Krebs to clinic: glutamine metabolism to cancer therapy, *Nat. Rev. Cancer*, 2016, **16**, 619–634.
15 A. D. Marshall, M. van Geldermalsen, N. J. Otte, T. Lum, M. Vellozzi, A. Thoeng, A. Pang, R. Nagarajah, B. Zhang, Q. Wang, L. Anderson, J. E. J. Rasko and J. Holst, ASCT2 regulates glutamine uptake and cell growth in endometrial carcinoma, *Oncogenesis*, 2017, **6**, e367.
16 Q. Wang, K. A. Beaumont, N. J. Otte, J. Font, C. G. Bailey, M. van Geldermalsen, D. M. Sharp, J. C. Tiffen, R. M. Ryan, M. Jormakka, N. K. Haass, J. E. J. Rasko and J. Holst, Targeting glutamine transport to suppress melanoma cell growth, *Int. J. Cancer*, 2014, **135**, 1060–1071.
17 C. Grewer and E. Grabsch, New inhibitors for the neutral amino acid transporter ASCT2 reveal its Na-dependent anion leak, *J. Physiol.*, 2004, **557**, 747–759.
18 M. L. Schulte, A. Fu, P. Zhao, J. Li, L. Geng, S. T. Smith, J. Kondo, R. J. Coffey, M. O. Johnson, J. C. Rathmell, J. T. Sharick, M. C. Skala, J. A. Smith, J. Berlin, M. K. Washington, M. L. Nickels and H. C. Manning, Pharmacological blockade of ASCT2-dependent glutamine transport leads to antitumor efficacy in preclinical models, *Nat. Med.*, 2018, **24**, 194–202.
19 Y. Kanai, B. Clémençon, A. Simonin, M. Leuenberger, M. Lochner, M. Weisstanner and M. A. Hediger, The SLC1 high-affinity glutamate and neutral amino acid transporter family, *Mol. Aspects Med.*, 2013, **34**, 108–120.
20 C. C. Huang, C. Q. Zhao, Q. Q. Deng, H. C. Zhang, J. S. Ren, D. Q. Yu and X. G. Qu, Hydrogen-bonded organic framework-based bioorthogonal catalysis prevents drug metabolic inactivation, *Nat. Catal.*, 2023, **6**, 729–739.
21 J. Konč, V. Sabatino, E. Jiménez-Moreno, E. Latocheski, L. R. Pérez, J. Day, J. B. Domingos and G. J. L. Bernardes, Controlled In-Cell Generation of Active Palladium(0) Species for Bioorthogonal Decaging, *Angew. Chem., Int. Ed.*, 2022, **61**, e202113519.
22 E. V. Y. Y. Xue, A. C. K. Lee, K. T. Chow and D. K. P. Ng, Promotion and Detection of Cell-Cell Interactions through a Bioorthogonal Approach, *J. Am. Chem. Soc.*, 2024, **146**, 17334–17347.

23 R. H. Zhao, Y. H. Chen and Y. Liang, Bioorthogonal Delivery of Carbon Disulfide in Living Cells, *Angew. Chem., Int. Ed.*, 2024, **63**, e202400020.
24 Y. X. Wang, D. Torres-García, T. P. Mostert, L. Reinalda and S. I. Van Kasteren, A Bioorthogonal Dual Fluorogenic Probe for the Live-Cell Monitoring of Nutrient Uptake by Mammalian Cells, *Angew. Chem., Int. Ed.*, 2024, **63**, e202401733.
25 X. Liu, T. Huang, Z. Chen and H. Yang, Progress in controllable bioorthogonal catalysis for prodrug activation, *Chem. Commun.*, 2023, **59**, 12548–12559.
26 F. Zeng, Y. Pan, M. Wu, Q. Lu, S. Qin, Y. Gao, X. Luan, R. Chen, G. He, Y. Wang, B. He, Z. Chen and Y. Song, Self-Metallized Whole Cell Vaccines Prepared by Microfluidics for Bioorthogonally Catalyzed Antitumor Immunotherapy, *ACS Nano*, 2024, **18**, 7923–7936.
27 W. J. Wang, X. Z. Zhang, R. Huang, C. M. Hirschbiegel, H. S. Wang, Y. Ding and V. M. Rotello, Activation of therapeutics through bioorthogonal catalysis, *Adv. Drug Delivery Rev.*, 2021, **176**, 113893.
28 Y. You, Q. Deng, Y. Wang, Y. Sang, G. Li, F. Pu, J. Ren and X. Qu, DNA-based platform for efficient and precisely targeted bioorthogonal catalysis in living systems, *Nat. Commun.*, 2022, **13**, 1459.
29 L. Y. Wu, H. H. Lin, X. Cao, Q. Tong, F. Q. Yang, Y. X. Miao, D. J. Ye and Q. L. Fan, Bioorthogonal Cu Single-Atom Nanozyme for Synergistic Nanocatalytic Therapy, Photothermal Therapy, Cuproptosis and Immunotherapy, *Angew. Chem., Int. Ed.*, 2024, **63**, e202405937.
30 Y. G. Bai, J. F. Chen and S. C. Zimmerman, Designed transition metal catalysts for intracellular organic synthesis, *Chem. Soc. Rev.*, 2018, **47**, 1811–1821.
31 J. Konc, V. Sabatino, E. Jiménez-Moreno, E. Latocheski, L. R. Pérez, J. Day, J. B. Domingos and G. J. L. Bernardes, Controlled In-Cell Generation of Active Palladium(0) Species for Bioorthogonal Decaging, *Angew. Chem., Int. Ed.*, 2022, **61**, e202113519.
32 M. Sancho-Albero, B. Rubio-Ruiz, A. M. Pérez-López, V. Sebastián, P. Martín-Duque, M. Arruebo, J. Santamaría and A. Unciti-Broceta, Cancer-derived exosomes loaded with ultrathin palladium nanosheets for targeted bioorthogonal catalysis, *Nat. Catal.*, 2019, **2**, 864–872.
33 T. Mirkovic, E. E. Ostroumov, J. M. Anna, R. van Grondelle Govindjee and G. D. Scholes, Light Absorption and Energy Transfer in the Antenna Complexes of Photosynthetic Organisms, *Chem. Rev.*, 2016, **117**, 249–293.
34 K. K. Sakimoto, A. B. Wong and P. D. Yang, Self-photosensitization of nonphotosynthetic bacteria for solar-to-chemical production, *Science*, 2016, **351**, 74–77.
35 S. Kalathil, M. Miller and E. Reisner, Microbial Fermentation of Polyethylene Terephthalate (PET) Plastic Waste for the Production of Chemicals or Electricity, *Angew. Chem., Int. Ed.*, 2022, **61**, e202211057.
36 X. M. Liu, T. Ueki, H. Y. Gao, T. L. Woodard, K. P. Nevin, T. D. Fu, S. Fu, L. Sun, D. R. Lovley and J. Yao, Microbial biofilms for electricity generation from water evaporation and power to wearables, *Nat. Commun.*, 2022, **13**, 4369.
37 B. C. Cao, Z. P. Zhao, L. L. Peng, H. Y. Shiu, M. N. Ding, F. Song, X. Guan, C. K. Lee, J. Huang, D. Zhu, X. Y. Fu, G. C. L. Wong, C. Liu, K. Nealson, P. S. Weiss, X. F. Duan and Y. Huang, Silver nanoparticles boost charge-extraction efficiency in Shewanella microbial fuel cells, *Science*, 2021, **373**, 1336–1340.
38 Q. W. Chen, J. W. Wang, X. N. Wang, J. X. Fan, X. H. Liu, B. Li, Z. Y. Han, S. X. Cheng and X. Z. Zhang, Inhibition of Tumor Progression through the Coupling of Bacterial Respiration with Tumor Metabolism, *Angew. Chem., Int. Ed.*, 2020, **59**, 21562–21570.
39 O. Felfoul, M. Mohammadi, S. Taherkhani, D. de Lanauze, Y. Z. Xu, D. Loghin, S. Essa, S. Jancik, D. Houle, M. Lafleur, L. Gaboury, M. Tabrizian, N. Kaou, M. Atkin, T. Vuong, G. Batist, N. Beauchemin, D. Radzioch and S. Martel, Magneto-aerotactic bacteria deliver drug-containing nanoliposomes to tumour hypoxic regions, *Nat. Nanotechnol.*, 2016, **11**, 941–947.
40 S. G. Ahmed, G. Oliva, M. L. Shao, X. H. Wang, J. J. Mekalanos and G. J. Brenner, Intratumoral injection of schwannoma with attenuated induces antitumor immunity and controls tumor growth, *Proc. Natl. Acad. Sci. U. S. A.*, 2022, **119**, e2202719119.
41 Y. H. Chen, M. Du, Z. Yuan, Z. Y. Chen and F. Yan, Spatiotemporal control of engineered bacteria to express interferon-γ by focused ultrasound for tumor immunotherapy, *Nat. Commun.*, 2022, **13**, 4468.
42 D. W. Zheng, Y. Chen, Z. H. Li, L. Xu, C. X. Li, B. Li, J. X. Fan, S. X. Cheng and X. Z. Zhang, Optically-controlled bacterial metabolite for cancer therapy, *Nat. Commun.*, 2018, **9**, 1680.
43 S. S. Lin, F. Wu, Y. F. Zhang, H. Chen, H. Y. Guo, Y. M. Chen and J. Y. Liu, Surface-modified bacteria: synthesis, functionalization and biomedical applications, *Chem. Soc. Rev.*, 2023, **52**, 6617–6643.
44 W. Lin, Y. Liu, J. Wang, Z. Zhao, K. Lu, H. Meng, R. Luoliu, X. He, J. Shen, Z. W. Mao and W. Xia, Engineered Bacteria Labeled with Iridium(III) Photosensitizers for Enhanced Photodynamic Immunotherapy of Solid Tumors, *Angew. Chem., Int. Ed.*, 2023, **62**, 202310158.
45 K. K. Liu, L. N. Wang, J. Peng, Y. Lyu, Y. M. Li, D. Y. Duan, W. Y. Zhang, G. J. Wei, T. P. Li, Y. J. Niu and Y. Zhao, Drug-Loaded Bacillus Calmette–Guérin Bacteria for Immuno-Chemo Combo Therapy in Bladder Cancer, *Adv. Mater.*, 2024, **36**, 2310735.
46 J. Lee, J. Y. Jang, M. S. Kwon, S. K. Lim, N. Kim, J. Lee, H. K. Park, M. Yun, M. Y. Shin, H. E. Jo, Y. J. Oh, B. H. Ryu, M. Y. Ko, W. Joo and H. J. Choi, Mixture of Two Strains Modulates the Gut Microbiota Structure and Regulatory T Cell Response in Diet-Induced Obese Mice, *Mol. Nutr. Food Res.*, 2018, **62**, 1800329.
47 Y. Wang, Y. You, Y. Tian, H. Y. Sun, X. Li, X. J. Wang, Y. H. Wang and J. S. Liu, PP04 Ameliorates High-Fat Diet-Induced Hyperlipidemia by Regulating Lipid Metabolism in C57BL/6N Mice, *J. Agric. Food Chem.*, 2020, **68**, 15154–15163.
48 R. R. Rodrigues, M. Gurung, Z. P. Li, M. García-Jaramillo, R. Greer, C. Gaulke, F. Bauchinger, H. You, J. W. Pederson,

S. Vasquez-Perez, K. D. White, B. Frink, B. Philmus, D. B. Jump, G. Trinchieri, D. Berry, T. J. Sharpton, A. Dzutsev, A. Morgun and N. Shulzhenko, Transkingdom interactions between and hepatic mitochondria attenuate western diet-induced diabetes, *Nat. Commun.*, 2021, **12**, 101.

49 Y. L. Shen, L. Q. Zhang, Y. Yang, B. C. Yin, B. C. Ye and Y. Zhou, Advances in the role and mechanism of lactic acid bacteria in treating obesity, *Food Bioeng.*, 2022, **1**, 101–115.

50 C. Hu, L. Cai, S. Liu and M. Pang, Integration of a highly monodisperse covalent organic framework photosensitizer with cation exchange synthesized Ag2Se nanoparticles for enhanced phototherapy, *Chem. Commun.*, 2019, **55**, 9164–9167.

51 F. M. Wang, Y. Zhang, Z. Du, J. S. Ren and X. G. Qu, Designed heterogeneous palladium catalysts for reversible light-controlled bioorthogonal catalysis in living cells, *Nat. Commun.*, 2018, **9**, 1209.

52 Z. M. Geng, Z. P. Cao, R. Liu, K. Liu, J. Y. Liu and W. H. Tan, Aptamer-assisted tumor localization of bacteria for enhanced biotherapy, *Nat. Commun.*, 2021, **12**, 6584.

53 M. J. Rong, J. Liu, Z. Sun, T. Li, Y. Li, C. H. Jiang and L. H. Lu, Rational Utilization of Black Phosphorus Nanosheets to Enhance Palladium-Mediated Bioorthogonal Catalytic Activity for Activation of Therapeutics, *Angew. Chem., Int. Ed.*, 2023, **62**, e202216822.

54 R. V, V. Gujar, H. Pathan, S. Islam, M. Tawre, K. Pardesi, M. K. Santra and D. Ottoor, Bioimaging Applications of Carbon dots (C. dots) and its Cystamine Functionalization for the Sensitive Detection of Cr(VI) in Aqueous Samples, *J. Fluoresc.*, 2019, **29**, 1381–1392.

55 M. van Geldermalsen, L.-E. Quek, N. Turner, N. Freidman, A. Pang, Y. F. Guan, J. R. Krycer, R. Ryan, Q. Wang and J. Holst, Benzylserine inhibits breast cancer cell growth by disrupting intracellular amino acid homeostasis and triggering amino acid response pathways, *BMC Cancer*, 2018, **18**, 689.